RESEARCH ARTICLE-PHYSICS

Investigation of the Microstructural, Morphological, and Magnetic Properties of Mechanically Alloyed $Co_{60}Fe_{18}Ti_{18}Si_4$ Powders

Hakan Yaykasli[1] · Baris Avar[2] · Mrutyunjay Panigrahi[3] · Musa Gogebakan[4] · Hasan Eskalen[5]

Abstract

Recently, there has been an increasing demand for Co-based alloys in modern industrial applications because of their excellent magnetic properties. Therefore, given the importance of obtaining high-quality Co-based alloy, such as $Co_{60}Fe_{18}Ti_{18}Si_4$ (at%), was synthesized using the mechanical alloying (MA) process. The research concerned the microstructural, morphological, and magnetic properties evolution of $Co_{60}Fe_{18}Ti_{18}Si_4$ (at%) alloy powders synthesized by MA in a high-energy planetary ball mill under argon (Ar) atmosphere, at a speed of 300 rpm. X-ray diffraction (XRD), scanning electron microscopy (SEM), transmission electron microscopy, and vibrating sample magnetometer analysis were employed to characterize different alloy powdered samples as a function of MA time (10 min–50 h). The XRD result indicates that the synthesized Co-based alloy powder has a widened peak of bcc-(Co, Fe, Ti, Si) solid solution appeared after 50 h of milling time. The crystallite and the lattice strain were achieved to about 8 nm and 1.235%, respectively, after 50 h of milling time. The average particle size was obtained to about 2.727 μm after 50 h of milling time, as observed from SEM analysis. From the VSM analysis, it was observed that the synthesized alloy powders show soft ferromagnetic behaviour. After 50 h of milling time, the magnetic saturation and the coercivity were attained to about 89.68 emu/g and 155.08 Oe, respectively.

Keywords Co-based alloy · Mechanical alloying · Nanocrystalline · Soft magnetic properties

1 Introduction

Cobalt-based alloys are requisite in the evolution progress of industry, and therefore, attraction in the investigation of these alloys has expanded. Co-alloys are usually preferred, such as industrial, aviation, and data storage, due to their soft magnetic behaviour, wear strength, and hardness [1]. These

✉ Baris Avar
  barisavar@beun.edu.tr,barisavar@gmail.com

1 Department of Electronic, Elbistan Vocational School of Higher Education, Kahramanmaras Istiklal University, Kahramanmaraş, Turkey

2 Department of Metallurgical and Materials Engineering, Zonguldak Bulent Ecevit University, 67100 Incivez, Zonguldak, Turkey

3 School of Mechanical Engineering, Vellore Institute of Technology, Chennai, Tamil Nadu 600127, India

4 Department of Physics, Kahramanmaras Sutcu Imam University, 46100 Kahramanmaraş, Turkey

5 Department of Opticianry, Vocational School of Health Services, Kahramanmaras Sutcu Imam University, Kahramanmaraş, Turkey

alloys can be produced in different forms by various methods, such as arc melting, melt spinning, mechanical alloying, etc. [2]. Mechanical alloying (MA) is the preferred technique for producing nanocrystalline and amorphous alloys [3]. On the other hand, Co-based alloys containing metalloids like boron (B) and silicon (Si) also have high melting points and commonly produce a homogeneous melt with these elements. Therefore, the MA technique is preferred, which does not require melting [4, 5].

Several types of research have been conducted on many Co-based alloys using the MA process in recent years. Wu et al. synthesized $Co_{62-X}Fe_XM_8B_{30}$ (M = Ti, Zr and x = 0, 5, 10, 15, 20, and 25) alloys by ball milling, and their magnetic behaviour has examined [6]. It has been reported that the saturation magnetization increases as the quantity of Fe addition in Co–Fe–B alloys. Hajipour et al. have explored the structural, magnetic, and thermal properties of Co-based $Co_{64}Fe_{21}Zr_{10}Cu_5$ alloy produced by ball milling [7]. After 10 h of milling, it was observed that a solid solution with an iron (Fe)-based, soft ferromagnetic behaviour, and the crystallite size value was attained to approximately

🍂 Springer

12.5 nm. Apart from this, other studies such as synthesis of $Co_{60}Fe_5Ni_5Ti_{25}B_5$ (at%) [8], $Co_{65}Ti_{25}W_5B_5$ (at%) [9], $Co_{78}B_{11}Si_{11}$ [10], $(FeCoNi)_{70}Ti_{10}B_{20}$ [11], $Co_{71}Ti_{24}B_5$ [12], $Co_{50}Fe_{21}Ti_{19}Ta_5B_5$ [13], $Co_{70}Fe_4Ni_2Si_{15}B_9$ [14], $Co_{62}Nb_6Zr_2B_{30}$ [15], and $Co_{40}Fe_{22}Ta_8B_{30}$ [16] alloy powders and the effect of their microstructural and magnetic properties, and mechanical alloying and the results were discussed.

It was observed from the above that various amorphous and nanocrystalline magnetic materials have been evolved by a combination of late transition metals like Co, Fe, Cr, and Ni, etc., early transition metals like Ti, Zr, Sc, and Nb, etc., and metalloids like B, P, Si, and As, etc. [11]. Keeping in mind, this study investigates the microstructural, thermal, and magnetic properties of $Co_{60}Fe_{18}Ti_{18}Si_4$ (at%) alloy powders, synthesized using a MA process at various milling times (10 min, and 1 h, 5 h, 10 h, 20 h, 30 h, and 50 h). While considering the strategy of the Co-based alloy design, titanium (Ti) was considered for better strength and improvement of the corrosion resistance. However, the addition of silicon (Si) shows excellent soft magnetic properties. The late transition metal like iron (Fe) was opted to increase the saturation magnetization and decrease the total cost of the Co-based alloy powder.

2 Experimental Procedure

The $Co_{60}Fe_{18}Ti_{18}Si_4$ (at%) alloy powders were synthesized by mechanical milling (10 min, and 1 h, 5 h, 10 h, 20 h, 30 h, and 50 h) in a planetary mill Fritsch Pulverisette 5. The experimental study used Co, Fe, Ti, and Si elemental powders, which have a purity of < 99.5% and particle size of < 100 μm purchased from Alfa Aesar. The powders were accurately weighed in a glove box filled with argon (Ar) gas. The powders were mixed to obtain the nominal atomic (at%) composition. Also, the cover of vials was taped with parafilm to keep away from oxidation. The grinding process of the alloy powder was used in a 250-mL stainless steel jar. The ratio of grinding balls to powder was determined as 20:1. In the initial conditions, a total of 15 g of powder were operated with mixed-sized balls of stainless steel containing 6 mm and 15 mm diameters. The rotation speed of the ball milling process was kept at 300 rpm and additionally stopped after 30 min of operation; it was stopped for 30 min to prevent overheating. To avoid the clump of the powders during the grinding process, benzene (C_6H_6) was chosen as a process control agent (PCA).

The crystallographic properties of the alloy powders were investigated by using Cu Kα radiation (λ = 0.15406 nm) X-ray diffraction (X'Pert PRO, Malvern PANalytical). The morphology and structure of the alloy powders were analyzed by scanning electron microscopy (SEM, ZEISS EVO LS10).

Moreover, the alloy powder's detailed microstructures were studied by transmission electron microscopy (JEOL JEM 2100 (UHR)). The magnetic properties of the milled alloy powders were analyzed at room temperature using the vibrating sample magnetometer (VSM) (Lake Shore 7407 model) within ± 200,00 Oe magnetic field ranges.

3 Results and Discussion

3.1 Phase Identification

X-ray diffraction measurement was used to investigate the crystal structure of mechanically alloyed $Co_{60}Fe_{18}Ti_{18}Si_4$ (at%) powders. Figure 1 illustrates the XRD pattern of the mechanically alloyed powders synthesized after 10 min and 1, 5, 10, 20, 30, and 50 h of milling. The XRD patterns revealed the appearance of the constituent elemental phases of two allotropic structures of Co (hcp: ICDD ref. code 00-001-1278) and Co (fcc: ICDD ref. code 00-015-0806), Fe (bcc: ICDD ref. code 01-087-0721), Ti (hcp: ICDD ref. code 00-044-1294), and Si (fcc: ICDD ref. code 01-075-0589) after 10 min of milling (Fig. 1a). After 10 min of milling (Fig. 1a), it was observed that the peaks were crystalline in nature. However, the intensities of the crystalline peaks were excessively decreased, and the peaks became slightly wider after increasing the milling time up to 1 h (Fig. 1b). This is because of the effect of the initiation of the lattice strain and the crystallite size refinement, which indicates the decreasing of the grain size during the MA process [13]. It was observed from the XRD patterns that both phases (fcc and hcp) coexisted in the sample milled for 10 min. Although the fcc phase is thermodynamically stable at > 450 °C and the hcp phase at < 450 °C, Dinega et al. reported that the fcc phase may be appeared at room temperature and even below room temperature in the case of nanoscale particles [17, 18]. Both phases of Co are close-packed structures that differ only in the stacking sequence of atomic planes in the [111] direction. The low activation energy for the formation of stacking faults often leads to the formation of both phases in the same sample under high-temperature crystallization techniques. The existence of both phases was first reported by Hull in 1921 after analyzing the XRD diffraction pattern of metallic Co powders prepared by several methods [19]. A similar observation has been noticed by Eskalen et al. and Hajipour et al. [4, 7]. After 5 h of milling (Fig. 1c), the Ti and the Si peaks completely disappeared, and one predominant peak and two small peaks appeared at $2\theta \approx 44.5°$, 64.9°, and 82.2°, respectively. Therefore, it indicates that the alloying of Fe and Ti with Co reached saturation and exhibits the feature of the (Fe, Co) solid solution behaviour, which initiates to occur [4, 7, 13, 20–29]. The Ti peak has vanished at the beginning of the milling stage, which can be ascribed to the
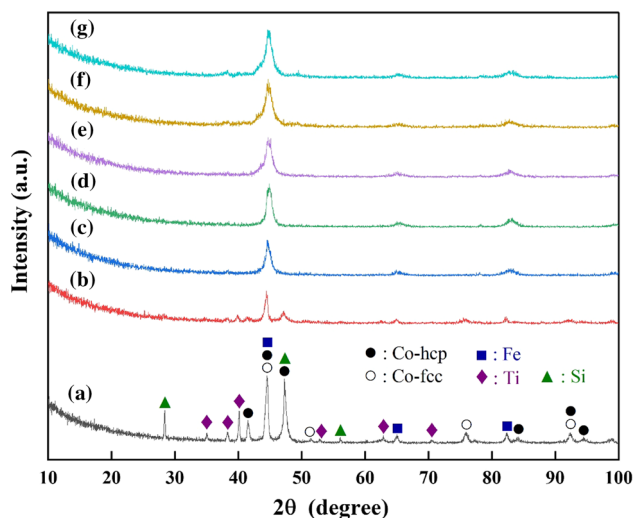
Fig. 1 The XRD patterns of mechanically alloyed $Co_{60}Fe_{18}Ti_{18}Si_4$ (at%) powders after **a** 10 min, **b** 1 h, **c** 5 h, **d** 10 h, **e** 20 h, **f** 30 h, and **g** 50 h of milling

Table 1 The mixing enthalpies among various atomic pairs of binary elements [32, 33]

Elements	Co	Fe	Ti	Si
Co	–	– 1	– 28	– 38
Fe	– 1	–	– 17	– 35
Ti	– 28	– 17	–	– 66
Si	– 38	– 35	– 66	–

substitutional dissolution of Ti into the lattice structure of (Fe, Co) alloy. The atomic size of Ti (0.293 nm) is more significant than that of Fe (0.254 nm) and Co (0.252 nm) elements, which causes the lattice structure size to grow, resulting in the movement of the dominant diffraction peak slightly toward a higher angle after 5 h of milling time [7]. There was no remarkable observation in the XRD pattern after milling the $Co_{60}Fe_{18}Ti_{18}Si_4$ (at%) powders for 10–50 h (Fig. 1d–g). However, the diffraction peaks were shifted slightly toward the higher angle and this is because of the lattice constriction that basically takes place within the solid solution process of Co-rich alloy [4, 6, 7, 23]. Finally, a Co-rich structure with bcc-(Co, Fe, Ti, Si) solid solution was existed in the structure with a slightly widened peak after 50 h of milling time (Fig. 1g). A similar observation has been noticed by Hajipour et al. [7]. Hajipour et al. noticed that after 2 h of milling [$(Co_{75}Fe_{25})_{85}Zr_{10}Cu_5$] (at%), the intensity of the peaks was reduced. The Co (fcc) phase has vanished, and Co (hcp) phase as the dominant diffraction peak remains, which can be ascribed to the allotropic transformation of element Co [7]. During the milling process, the dissolution of constituent elements to the evolution of a solid solution phase and remarkable severe plastic deformation was noticed [7]. However, Eskalen et al. reported that both phases (fcc and hcp) coexisted in the sample ($Co_{60}Fe_{18}Ti_{18}B_4$) alloy powder and milled for 50-h [4].

The mixing enthalpies among various atomic pairs of binary elements are presented in Table 1. The dissolution of the elements is more achievable because of the thermodynamic force that results from the negative heat of mixing among the elements. According to Schwarz et al., the larger negative heat of mixing between the elements (Table 1) can

provide the required thermodynamic driving force for the inter-diffusion of the various elements and solid-state amorphization [7, 13, 30].

The evolution of the amorphous phase in the $Co_{60}Fe_{18}Ti_{18}Si_4$ (at%) alloy powders during MA can be investigated based on the thermodynamic aspect. The amorphous phase is thermodynamically more stable with respect to the corresponding solid solution if the change in Gibbs free energy for amorphization becomes more negative than that of the solid solution. The change in Gibbs free energy for a reaction is described using Eq. (1).

$$\Delta G = \Delta H - T \Delta S \tag{1}$$

where ΔH is the total enthalpy change and ΔS is the entropy of mixing.

The ΔS can be determined (for an ideal solid solution) using Eq. (2) [13].

$$\Delta S = - R \sum_{1}^{n} x_i \ln x_i \tag{2}$$

where R, x_i, and n are the universal gas constant, the molar fraction of element i, and a number of elements, respectively.

The total mixing enthalpy changes, ΔH, based on Miedema's semi-empirical model can be expressed using Eq. (3) [13, 30–33].

$$\Delta H = \Delta H_{chemical} + \Delta H_{elastic} + \Delta H_{structural} \tag{3}$$

where $\Delta H_{chemical}$, $\Delta H_{elastic}$, and $\Delta H_{structural}$ are the chemical contribution created by mixing the constituents, the elastic enthalpy variations derived from the size mismatch of the elements, and the structural enthalpy change originating from the difference in valence electrons and crystal structure of solvent and solute atoms, respectively.

The elements such as Ti and Si possess a greater potential to dissolve into the other elements such as Co and Fe because of the more negative heat of mixing as compared to Co and Fe [32, 33]. Therefore, it was dissolved in the bcc-(Co, Fe) structure at the beginning stage of the milling process, and with increasing the milling time up to 50 h, the peaks of Ti
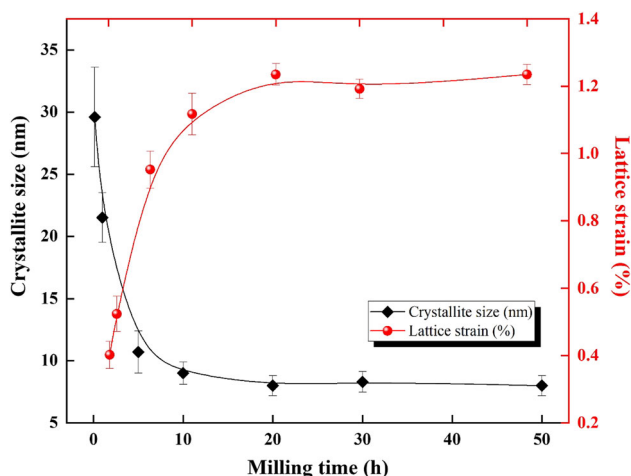
Fig. 2 Variation of average crystallite size and lattice strain as a function of milling time

and Si disappeared, and the widened peak of bcc-(Co, Fe, Ti, Si) solid solution remains [7].

The average crystallite size and lattice strain of the $Co_{60}Fe_{18}Ti_{18}Si_4$ (at%) alloy powders as a function of various milling times are shown in Fig. 2. It was clearly observed that a remarkable decrease in crystallite size is accompanied by a rise in the lattice strain as the milling time progresses. The average crystallite size (D) of the $Co_{60}Fe_{18}Ti_{18}Si_4$ (at%) alloy powders as a function of various milling times was obtained using Scherrer's Eq. (4) [25, 34, 35].

$$D = \frac{k\lambda}{\beta\cos`} \tag{4}$$

where k, λ, β, and cos are the shape factors commonly considered as a unity, the X-ray wavelength, the full width at half maximum in radians, and Bragg angle, respectively.

The microstrain was calculated by using following Eq. (5) [27, 34, 35].

$$\varepsilon = \frac{\beta}{4\tan\theta} \tag{5}$$

where θ is the position of the diffraction peak.

The crystallite size and lattice strain calculation have been explained in detail in our earlier paper [34]. The crystallite size was around 29.6 nm after 10-min milling of the powders. However, it was sharply reduced to 9 nm after 10-h milling. The crystallite size (8 nm) remained stable after 50-h milling. However, the degree of thermodynamic stability can differ during the milling process, creating phase transformation to take place [7], while the lattice strain increases rapidly with the increasing milling time from 10 min (0.402%) to 10 h (1.117%) of milling. The rise of lattice strain is because of the formation of grain boundaries along with the lattice defects and dislocations generated by the milling process [28, 36].

On longer milling time up to 50 h, the increase in the lattice strain was slow, and it reached a value of 1.235% finally. The lattice strains in crystalline grains arise from different origins like thermal expansions, contractions, vacancies, dislocations, shear planes, etc. [37]. In addition, Koohkan et al. observed that the rise in residual strains inside the crystallite could be because of the stress fields connected with the multiplication of the dislocations [23, 28, 36, 37]. On the contrary, Lachheb et al. concluded that the alteration of the chemical composition of the powder mixture at the nanoscale range ensures the evolution of solid substitution solutions which creates a significant character in the alteration of microstructural variables about the crystallite size and microstrains [38].

3.2 SEM and TEM Analysis

SEM was employed to observe the morphological development of the mechanically alloyed $Co_{60}Fe_{18}Ti_{18}Si_4$ (at%) powders after 10 min and 1, 1.5, 10, 20, 30, and 50 h of milling. Figure 3 illustrates the morphology of $Co_{60}Fe_{18}Ti_{18}Si_4$ (at%) alloy powders as a function of various milling times. After 10 min of milling (Fig. 3a), it shows a broad size distribution, with irregular geometries in the structure and particle sizes of the milled powder. This is associated with the starting conditions of the individual elemental powders with different geometries and particle sizes that tend to be agglomerated, flattened, and widened, which is a usual property of ductile particles [23]. This is because of the action of the compressive milling forces generated by repeated collisions that occur in the MA process. During the MA process, the powder particles are consistently conquered to the periodic consequences of fracture and welding, bringing to the evolution of aggregates whose particle size results from the competition among the above phenomena [23]. The development of the morphology of the powder particles during MA is linked to the variation between the mechanical properties of the distinct individual elements. Therefore, the size of the mechanically alloyed powders became smaller with the increase in the milling time up to 1 h (Fig. 3b). However, the SEM images display an enormous rise in particle size because of the evolution of agglomerates with irregular shapes as a result of the cold welding caused by the MA of 5h (Fig. 3c) and 10 h (Fig. 3d), respectively. The rise in particle size is ascribed to the ductile features of Co that incline them to become agglomerates. While the milling time was prolonged to 20 h (Fig. 3e), the agglomerates exhibit a decrease in particle size because of the particle deformation that generates strain hardening into the particles. Finally, after 30 and 50 h of milling ((Fig. 3f, g), the particle size was reduced, and the shape and size were semi-spherical and more uniform. This is generally due to the equilibrium between fracturing and cold-welding processes [5, 7, 25, 38].
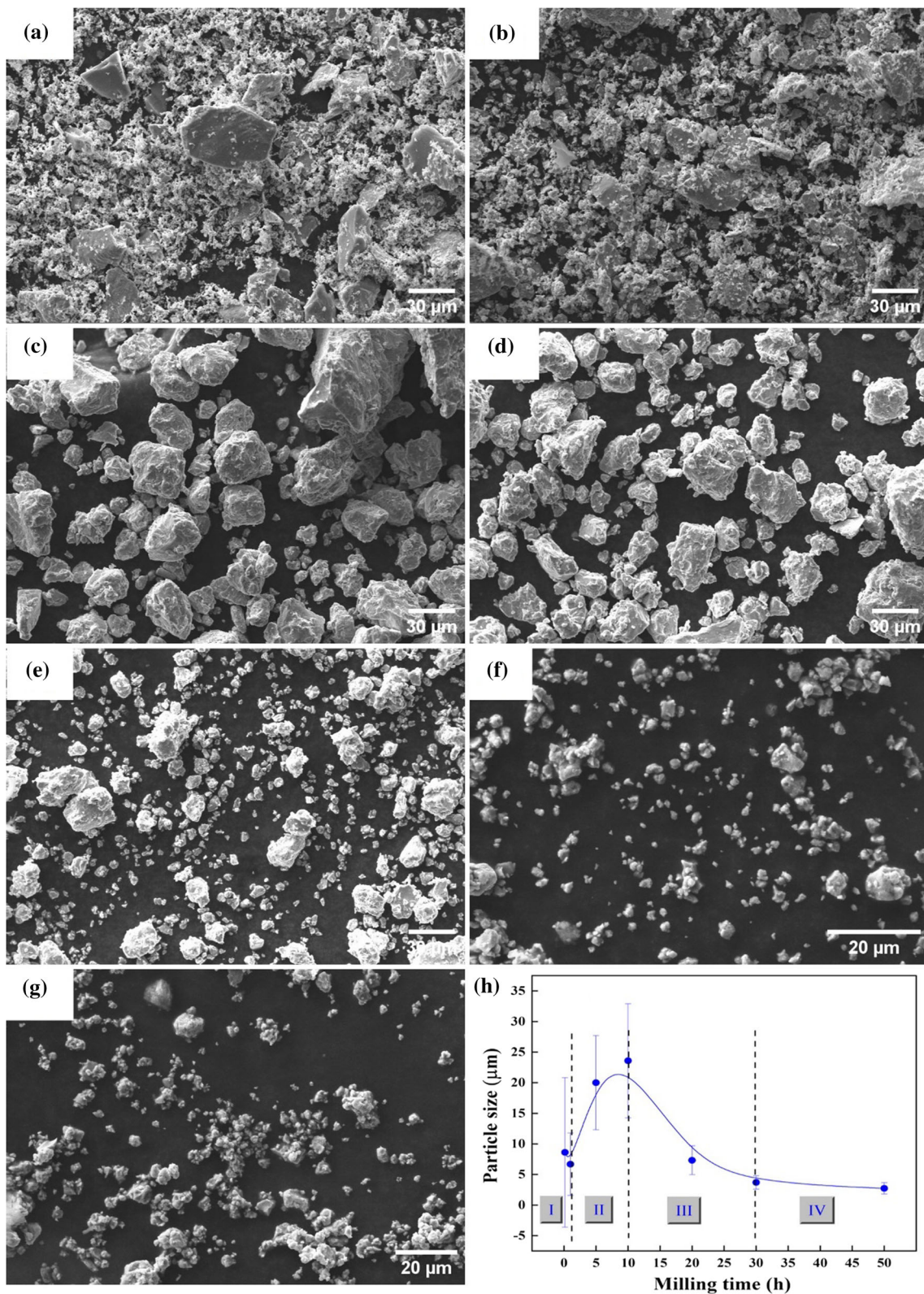
Fig. 3 SEM images of mechanically alloyed $Co_{60}Fe_{18}Ti_{18}Si_4$ (at%) powders after **a** 10 min, **b** 1 h, **c** 5 h, **d** 10 h, **e** 20 h, **f** 30 h, and **g** 50 h of milling, and **h** average particle size variation as a function of milling time
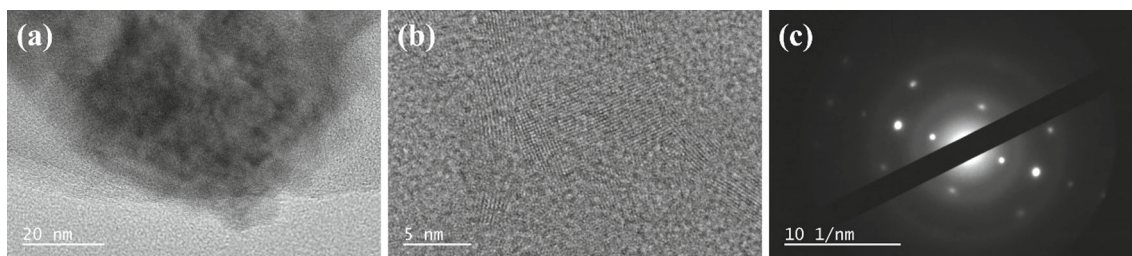
Fig. 4 **a**, **b** HRTEM images and **c** SAED image of the 50-h milled $Co_{60}Fe_{18}Ti_{18}Si_4$ (at%) powders

The development of the average particle size with respect to various milling times is shown in Fig. 3h. Generally, the cold working and the shear forces induced to design the form of particles during the milling process [7]. The size of the powder particle was calculated from the SEM micrographs using ImageJ tool software. The effect of milling time on particle size can be classified into four various stages [4]. In the first stage, the particle size was decreased up to 8.608 µm after 10 min of milling and reached a value of about 6.686 µm after 1 h of milling of powders. In the second stage, the particle size rose rapidly and reached about 23.585 µm with prolonged milling time up to 10 h. Then, in the third stage, the particle size was reduced drastically to 3.691 µm after 30 h of milling. Finally, in the last step, the particle size was further reduced to 2.727 µm after 50 h of milling and further remained stable.

The high-resolution transmission electron microscopy (HRTEM) images of 50-h milled powder sample was further investigated to have more details of structural properties. Figure 4 illustrates the TEM bright-field image and the corresponding selected area electron diffraction (SAED) pattern for the mechanically alloyed $Co_{60}Fe_{18}Ti_{18}Si_4$ (at%) powder sample achieved after 50 h of milling. The dark portion present in Fig. 4a was probably because the particles were agglomerated but not completely dispersed. The existence of lattice fringes was distinctly noticed through HRTEM (Fig. 4b). The average crystallite size was evaluated to be about 3 nm from the above. The SAED image (Fig. 4c) shows the nano-sized nature of the particles. The bright diffraction spots which were seen in the image (Fig. 4c) are ascribed to the crystalline phases, whereas the partially amorphous structure is illustrated by the diffused halo [4, 7]. The bright diffraction spots in the SAED pattern were deformed from circular shapes to elongated spots. This extension of the spots was ascribed to the generation of dislocations, leading to a change of crystal orientation in some particular portion of the crystal structure [7]. The diffraction rings are because of the powder sample's different directions of crystal structures [7, 25, 35]. Therefore, the SAED pattern is verified that the prepared powder sample has both an amorphous and crystalline structure. Accordingly, it can be presumed from the

TEM analysis that the achieved SAED pattern and the crystallite size through the HRTEM image proportionally agree with the XRD analysis.

3.3 Magnetic Properties

The hysteresis loops give essential particulars about the magnetic properties of the materials. Therefore, the VSM was used to analyze the mechanically alloyed $Co_{60}Fe_{18}Ti_{18}Si_4$ (at%) powders to study the magnetic behaviour with respect to different milling times. Figure 5a illustrates the hysteresis loop (M: magnetization vs H: applied magnetic field) for the mechanically alloyed $Co_{60}Fe_{18}Ti_{18}Si_4$ (at%) powders with respect to different milling times by applying an external field between − 20,000 and + 20,000 Oe at 23 °C. As illustrated in Fig. 5a, the sigmoidal profile of the hysteresis loops and the Ms: saturation magnetization of the mechanically alloyed powders are impacted by the milling time. The inset in Fig. 5a indicates the dependence of M: magnetization at a limited range of external magnetic fields. As seen in Fig. 5a, all hysteresis loops exhibit soft ferromagnetic nature [7, 28, 34, 39–41]. However, it is demonstrated that the 50-h milled mechanically alloyed powder shows a relatively more minor loop area and coercive force, which is a significant aspect of soft magnetic materials. It was noticed that the mechanically alloyed $Co_{60}Fe_{18}Ti_{18}Si_4$ (at%) powders milled at 10 min–20 h are magnetically saturated at a magnetic field of about 9800 Oe, whereas saturation occurs for 30-h milled sample at a lower field of around 8200 Oe. However, the saturation occurs for a 50-h milled sample at an extensively lower field of about 2200 Oe. Alternatively, the powders that undergo a longer milling time represent a less tendency for a round-shaped hysteresis loop. This kind of behaviour shows the increased magnetic softness property or decreasing the shape anisotropy, caused by alterations in the morphology of the particle from flattened to semi-spherical shape (Fig. 3a–g) [13, 23, 31].

The magnetic anisotropy constant was calculated for the mechanically alloyed samples using the law of approach to saturation. The law of approach to saturation in highly anisotropic compounds has rarely been studied since their anisotropy fields are generally greater than 100,000 Oe and

the magnetic fields needed for the magnetization measurements are very large. According to the law above, the M: magnetization can be demonstrated with respect to the H: applied magnetic field in the saturation region using Eq. (6) [36, 39].

$$M = Ms\left(1 - \frac{a}{H} - \frac{b}{H^2}\right) + XH \qquad (6)$$

where MS is the saturation magnetization, b/H^2 is generated by uniform magneto-crystalline anisotropy, a/H is ascribed to the existence of structural defects and non-magnetic inclusions, and X is the high field susceptibility resulting from the enhancement in the saturation magnetization by the applied magnetic field. The term b can be demonstrated in terms of the first-order uniaxial magnetic anisotropy, K. In the case of a ferromagnet (cubic crystal structure), the term b can be calculated using Eq. (7) [36, 39].

$$b = \left(\frac{8}{105}\frac{K^2}{Ms^2}\right) \qquad (7)$$

where K is the cubic anisotropy constant of the first order.

From the magnetization loops analysis, K and Ms can be calculated using Eqs. 6 and 7.

Similarly, coercivity (Hc) is the main criterion like Ms for soft magnetic materials. Usually, impurities, pores, internal micro-strain, and defects influence Hc [36]. However, the crystallite size is the most influenced mechanism on Hc. Therefore, the Hc depends on the crystallite size (D) and the Ms, which can be calculated using Eq. (8) [25, 40].

$$Hc \approx 3\sqrt{\frac{KTcK_1}{aMs}\frac{1}{D}} \qquad (8)$$

where T_c is the Curie temperature, k is the Boltzmann constant, K_1 is the magnetocrystalline anisotropy, and a is the lattice constant.

Figure 5b indicates the saturation magnetization (Ms) and coercivity (Hc) of the mechanically alloyed $Co_{60}Fe_{18}Ti_{18}Si_4$ (at%) powders with respect to different milling times, and the Ms and Hc were achieved from the hysteresis loops. It was observed from Fig. 5b that the Ms value was decreased in the beginning from 142.83 to 140 emu/g (milling from 10 min to 1 h). This is because of the dissolution of non-ferromagnetic atoms such as Ti and Si in the mechanically alloyed structure [20]. The effect of Si by adding to the alloy powder is to increase the atomic percentage of non-magnetic elements. Therefore, it can result in decreasing the exchange interaction among ferromagnetic atoms. The same observation was noticed in the XRD results in Fig. 1b that the intensity of Ti and Si peaks was significantly decreased, which is a sign of dissolution of those elements. However, a significant
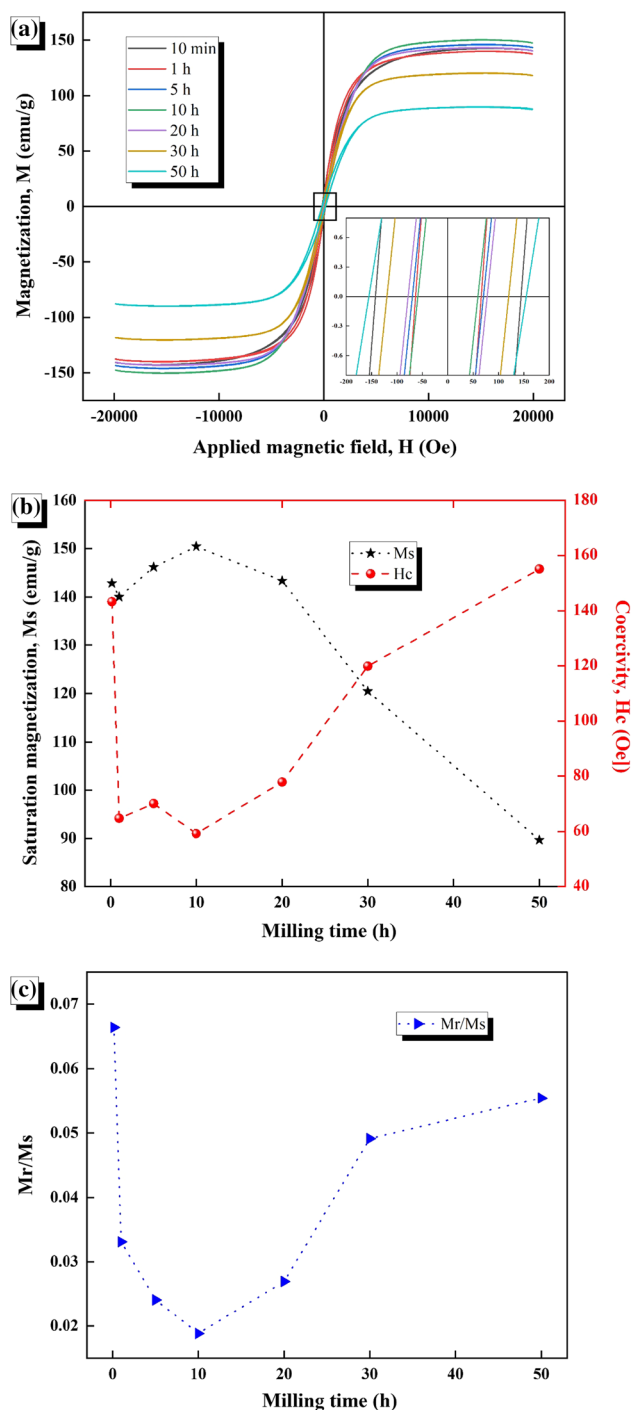

Fig. 5 Evolution of **a** the hysteresis curves, **b** saturation magnetization (Ms) and coercivity (Hc), and **c** remanence-to-saturation ratio (Mr/Ms) of the mechanically alloyed powder samples as a function of various milling time

increase in Ms (150.42 emu/g) was observed while milling up to 10 h. This is because of the decrease in magneto-crystalline anisotropy developed from grain refinement, and this leads to facile development of the magnetic direction of magnetic grains, which decreases the crystallite size (Fig. 2) at the initial stage of the milling process [7]. Finally, the Ms value was

decreased from 150.42 to 89.68 emu/g, while increasing the milling time from 10 to 50 h. This is because the decrease in grain size and structural distortions combined with interfaces decline the magnitude of Ms due to the variation of the interatomic spacing in the interfacial regions [23, 41]. The Hc value decreases from 143.32 to 59.23 Oe while milling from 10 min to 10 h, which is shown in Fig. 5b. This is because of the reduction in crystallite size and the increase in strain amid the alloying process that can decrease Hc at the beginning of the milling process. The same observation is noticed in Fig. 2. The Hc is also directly proportional to the residual stress [7, 40]. After prolonged the milling time up to 50 h, the Hc rose to 155.08 Oe because of the random anisotropy model. The soft magnetic property is associated with averaging out the magneto-crystalline anisotropy ascribed to the arbitrary disperse of the grains at the nanoscale level [7]. The remanence-to-saturation ratio (Mr/Ms) is a significant magnetic criterion in calculating the magnetic energy. Figure 5c shows the Mr/Ms for the $Co_{60}Fe_{18}Ti_{18}Si_4$ (at%) powders with respect to various milling times. The mechanically alloyed powder samples synthesized have a Mr/Ms ratio within the range of 0.019 and 0.067, which is indeed lesser than that anticipated for a single-domain particle. However, a single-domain crystal instinctively breaks into several domains, and this decreases the magnetization energy [23–25, 28, 34, 37, 40]. Hence, the crystallite favours abiding a single domain in a minute particle size. For mechanical alloying, the Mr/Ms value is generally small, at the range of 0.01 and 0.1, which was reported by Carrillo et al. [24]. A value adjacent to one (1) is generally appropriate for magnetic storage systems, while a value near zero (0) is acceptable for transformer cores [24].

4 Conclusions

The $Co_{60}Fe_{18}Ti_{18}Si_4$ (at%) alloy powders were successfully synthesized using a mechanical alloying process. The microstructural, morphological, magnetic properties, and the effect of the milling time were investigated in detail. It was observed that after 10 min of milling, the Bragg peaks were crystalline in behaviour, and while increasing the milling time (5 h), the Ti and Si peaks disappeared entirely. After 20-h milling time, the particle size was decreased due to severe plastic deformation and the dissolution of constituent elements in the formation of the solid solution phase. However, the particle size attained a saturated value after 30 h of milling, and a widened peak of bcc-(Co, Fe, Ti, Si) solid solution remained (after 50 h of milling) and confirmed the formation of $Co_{60}Fe_{18}Ti_{18}Si_4$ (at%) alloy. The crystallite size was decreased with respect to milling time from 29.6 nm (10 min of milling) to 8 nm (50 h of milling), whereas the microstrain was increased from 0.402% (10 min

of milling) to 1.235% (50 h of milling), respectively. SEM analysis has shown that the continuous transformation of the phases appeared, and the average particle size was decreased to 2.727 μm while prolonging milling time. The results also showed that the morphologies of the powders underwent fracturing and welding during the milling process. TEM analysis was conducted to analyze the structural property more in detail and the SAED pattern and the crystallite size through the HRTEM image supported the XRD analysis. The TEM results also show that the synthesized nanostructured powders have both amorphous and nanocrystalline phases. The soft ferromagnetic behaviour of the mechanically alloyed samples exhibited higher saturation magnetization (142.83 emu/g) at the beginning of the milling time (10 min). It was decreased to 89.68 emu/g while increasing the milling time up to 50 h. Similarly, the coercivity was about 143.32 Oe in the initial milling time of 10 min, whereas it was increased up to 155.08 Oe while prolonged the milling time (50 h). It was also observed that the mechanically alloyed powders have a Mr/Ms ratio within the range of 0.019 and 0.067, which were calculated with respect to different milling times.

Declarations

Conflict of interest The authors declare that there is no conflict of interest.

Consent to Participate The author signs for and accepts responsibility for releasing this material on behalf of all co-authors.

References

1. Molladavoudi, A.; Amirkhanlou, S.; Shamanian, M.; Ashrafizadeh, F.: Synthesis and characterization of nanocrystalline CoTi intermetallic compound prepared by mechanical alloying. Mater. Lett. **81**, 254–257 (2012). https://doi.org/10.1016/j.matlet.2012.04.104

2. Longhin, M.; Viennois, R.; Ravot, D.; Robin, J.; Papet, P.: Nanostructuration of CoSi by mechanical milling and mechanical alloying. Solid State Sci. **38**, 129–137 (2014). https://doi.org/10.1016/j.solidstatesciences.2014.10.011

3. Li, N.; Yin, F.; Feng, L.: Microstructure of a V-containing cobalt based alloy prepared by mechanical alloying and hot pressed sintering. Metals (Basel) (2019). https://doi.org/10.3390/met9040464

4. Eskalen, H.; Aslan, M.; Yaykaşlı, H.; Gögebakan, M.: Synthesis and characterization of Co–B–Fe–Ti nanosized alloyed powders. Int. J. Mater. Res. **112**, 35–41 (2021). https://doi.org/10.1515/ijmr-2020-7704

5. Eskalen, H.; Uruş, S.; Yaykaşlı, H.; Gögebakan, M.: Microstructural characterization of ball milled Co60 Fe18Ti18Nb4 alloys and

their photocatalytic performance. Alloy Mater. Their Allied Appl. (2020). https://doi.org/10.1002/9781119654919.ch6

6. Wu, H.-M.; Hu, C.-J.; Li, H.-C.: Formation of Co–Fe–M–B (M=Zr, Ti) amorphous powders by mechanical alloying and their magnetic properties. J. Alloys Compd. **483**, 553–556 (2009). https://doi.org/10.1016/j.jallcom.2008.07.195

7. Hajipour, M.; Raanaei, H.; Zarei, S.: Magnetic, morphological and thermal studies of nanostructured cobalt-based Co-Fe-Zr-Cu alloy prepared by mechanical alloying. J. Magn. Magn. Mater. **548**, 168992 (2021). https://doi.org/10.1016/j.jmmm.2021.168992

8. Avar, B.; Ozcan, S.: Characterization and amorphous phase formation of mechanically alloyed Co60Fe5Ni5Ti25B5 powders. J. Alloys Compd. **650**, 53–58 (2015). https://doi.org/10.1016/j.jallcom.2015.07.268

9. Avar, B.: Structural, thermal and magnetic characterization of nanocrystalline Co65Ti25W5B5 powders prepared by mechanical alloying. J. Noncryst. Solids. **432**, 246–253 (2016). https://doi.org/10.1016/j.jnoncrysol.2015.10.016

10. Pękała, M.; Jachimowicz, M.; Fadeeva, V.I.; Matyja, H.: Phase transformations in Co-B-Si alloys induced by high-energy ball milling. J. Noncryst. Solids. **287**, 360–365 (2001)

11. Avar, B.; Simsek, T.; Ozcan, S.; Chattopadhyay, A.K.; Kalkan, B.: Structural stability of mechanically alloyed amorphous (FeCoNi)70Ti10B20 under high-temperature and high-pressure. J. Alloys Compd. **860**, 158528 (2021). https://doi.org/10.1016/j.jallcom.2020.158528

12. El-Eskandarany, M.S.; Ishihara, S.; Zhang, W.; Inoue, A.: Fabrication and characterizations of new glassy Co71Ti24B5 alloy powders and subsequent hot pressing into a fully dense bulk glass. Metall. Mater. Trans. A **36**, 141–147 (2005). https://doi.org/10.1007/s11661-005-0146-8

13. Taghvaei, A.H.; Khoshrodi, A.M.: Characterization, thermodynamic analysis and magnetic investigation of new soft magnetic amorphous/nanocrystalline Co50Fe21Ti19Ta5B5 powders produced by mechanical alloying. J. Alloys Compd. **742**, 887–896 (2018). https://doi.org/10.1016/j.jallcom.2018.01.382

14. Neamţu, B.V.; Chicinaş, H.F.; Marinca, T.F.; Isnard, O.; Chicinaş, I.: Preparation and characterisation of Co–Fe–Ni–M–Si–B (M = Zr, Ti) amorphous powders by wet mechanical alloying. J. Alloys Compd. **673**, 80–85 (2016). https://doi.org/10.1016/j.jallcom.2016.02.233

15. Moreno, L.M.; Blázquez, J.S.; Ipus, J.J.; Conde, A.: Amorphization and evolution of magnetic properties during mechanical alloying of Co62Nb6Zr2B30: Dependence on starting boron microstructure. J. Alloys Compd. **585**, 485–490 (2014). https://doi.org/10.1016/j.jallcom.2013.09.191

16. Taghvaei, A.H.; Stoica, M.; Khoshkhoo, M.S.; Thomas, J.; Vaughan, G.; Janghorban, K.; Eckert, J.: Microstructure and magnetic properties of amorphous/nanocrystalline Co40Fe22Ta8B30 alloy produced by mechanical alloying. Mater. Chem. Phys. **134**, 1214–1224 (2012). https://doi.org/10.1016/j.matchemphys.2012.04.031

17. Dinega, D.P.; Bawendi, M.G.: A solution-phase chemical approach to a new crystal structure of cobalt. Angew. Chem. Int. Ed. **38**, 1788–1791 (1999). https://doi.org/10.1002/(SICI)1521-3773(19990614)38:12%3c1788::AID-ANIE1788%3e3.0.CO;2-2

18. Zhang, Z.; Budnick, J.I.; Hines, W.A.; Perry, D.M.; Wells, B.O.: Direct evidence for the source of reported magnetic behavior in "CoTe." AIP Adv. **7**, 125322 (2017). https://doi.org/10.1063/1.4997161

19. Hull, W.A.: X-ray crystal analysis of thirteen common metals. Phys. Rev. **17**, 571–588 (1921). https://doi.org/10.1103/PhysRev.17.571

20. Cotai, A.; Neamţu, B.V.; Popa, F.; Marinca, T.F.; Isnard, O.; Chicinaş, I.: Synthesis and characterization of amorphous Fe38.5Co38.5Nb7B15Cu1 powders via mechanosynthesis using

industrial raw materials. J. Alloys Compd. **880**, 160497 (2021). https://doi.org/10.1016/j.jallcom.2021.160497

21. Li, R.; Liu, X.; Yu, P.; Fan, X.; Tong, X.; Liu, Q.; Lu, Y.; Zhang, Y.; Li, G.: Synthesis and characterization of a ultrafine grained (CoCrFeNi)80Mn10Ti10 multi-principal element alloy nanocomposite. Mater. Sci. Eng. **833**, 142569 (2022). https://doi.org/10.1016/j.msea.2021.142569

22. Nascimento, L.: Evolution of the amorphous phase of the alloy Co67Nb25B17. Orbital Electron. J. Chem. **13**(1), 65–68 (2021)

23. Daly, R.; Khitouni, N.; Escoda, M.L.; Isern, N.L.; Jose, S.M.J.; Greneche, J.M.; Khitouni, M.: Microstructure, magnetic and mössbauer studies of mechanically alloyed FeCoNi nanocrystalline powders. Arab. J. Sci. Eng. **46**, 5633–5643 (2021). https://doi.org/10.1007/s13369-020-05166-2

24. Carrillo, A.; Daza, J.; Saurina, J.; Escoda, L.; Suñol, J.-J.: Structural, thermal and magnetic analysis of Fe75Co10Nb6B9 and Fe65Co20Nb6B9 nanostructured alloys. Materials **14**, 4542 (2021). https://doi.org/10.3390/ma14164542

25. Prasad, N.K.; Kumar, V.: Microstructure and magnetic properties of equiatomic FeNiCo alloy synthesized by mechanical alloying. J. Mater. Sci. Mater. Electron. **26**, 10109–10118 (2015). https://doi.org/10.1007/s10854-015-3695-7

26. Sourmail, T.: Near equiatomic FeCo alloys: constitution, mechanical and magnetic properties. Prog. Mater. Sci. **50**, 816–880 (2005). https://doi.org/10.1016/j.pmatsci.2005.04.001

27. Yaykaslı, H.; Eskalen, H.; Kavun, Y.; Gogebakan, M.: Microstructural, thermal, and radiation shielding properties of Al50B25Mg25 alloy prepared by mechanical alloying. J. Mater. Sci. Mater Electron. **33**, 2350–2359 (2022). https://doi.org/10.1007/s10854-021-07434-9

28. Panigrahi, M.; Avar, B.: Influence of mechanical alloying on structural, thermal, and magnetic properties of Fe50Ni10Co10Ti10B20 high entropy soft magnetic alloy. J Mater Sci. Mater Electron. **32**, 21124–21134 (2021). https://doi.org/10.1007/s10854-021-06612-z

29. Avar, B.; Panigrahi, M.; Soguksu, A.K.; Rajendrachari, S.; Gundes, A.: Photocatalytic activity of soft magnetic Fe80−xCoxZr10Si10 (x=0, 40, and 80) nanocrystalline melt-spun ribbons. Top. Catal. (2022). https://doi.org/10.1007/s11244-022-01569-7

30. Schwarz, R.; Johnson, W.: Formation of an amorphous alloy by solid-state reaction of the pure polycrystalline metals. Phys. Rev. Lett. **51**(5), 415–418 (1983). https://doi.org/10.1103/PhysRevLett.51.415

31. Taghvaeia, A.H.; Nickjeh, H.S.; Ramasamy, P.; Eckert, J.: Synthesis, thermodynamic analysis and magnetic study of novel ballmilled Co50Fe25Ta5Si5C15 glassy powders with high thermal stability. J. Alloys Compd. **894**, 162509 (2022). https://doi.org/10.1016/j.jallcom.2021.162509

32. Takeuchi, A.; Inoue, A.: Calculations of mixing enthalpy and mismatch entropy for ternary amorphous alloys. Mater. Trans. JIM **41**(11), 1372–1378 (2000). https://doi.org/10.2320/matertrans1989.41.1372

33. Takeuchi, A.; Inoue, A.: Classification of bulk metallic glasses by atomic size difference, heat of mixing and period of constituent elements and its application to characterization of the main alloying element. Mater. Trans. **46**(12), 2817–2829 (2005). https://doi.org/10.2320/matertrans.46.2817

34. Panigrahi, M.; Avar, B.: Development of microstructural and magnetic properties of Co50Si50 alloy powders during mechanical alloying approach. Appl. Phys. A **127**, 967 (2021). https://doi.org/10.1007/s00339-021-05121-4

35. Girman, V.; Lisnichuk, M.; Yudina, D.; Matvija, M.; Sovák, P.; Bednarcík, J.: Structural evolution in wet mechanically alloyed Co-Fe-(Ta, W)-B alloys. Metals **11**(5), 800 (2021). https://doi.org/10.3390/met11050800

36. Betancourt-Cantera, J.A.; Sánchez-De Jesús, F.; Bolarín-Miró, A.M.; Torres-Villasenor, G.; Betancourt-Cantera, L.G.: Magnetic properties and crystal structure of elemental cobalt powder modified by high-energy ball milling. J. Mater. Res. Technol. **8**(5), 4995–5003 (2019). https://doi.org/10.1016/j.jmrt.2019.07.048

37. Koohkan, R.; Sharafi, S.; Shokrollahi, H.; Janghorban, K.: Preparation of nanocrystalline Fe–Ni powders by mechanical alloying used in soft magnetic composites. J. Magn. Magn. Mater. **320**, 1089–1094 (2008). https://doi.org/10.1016/j.jmmm.2007.10.033

38. Lachheb, R.; Bachaga, T.; Makhlouf, T.; Khitouni, M.: Phase transformations and microstructural properties of nanocrystalline $Fe_{75}Si_{10}B_{10}Nb_5$ alloy synthesized by mechanical alloying. Adv. Powder Technol. **26**(6), 1563–1569 (2015). https://doi.org/10.1016/j.apt.2015.08.010

39. Andreev, S.V.; Bartashevich, M.I.; Pushkarsky, V.I.; Maltsev, V.N.; Pamyatnykh, L.A.; Tarasov, E.N.; Kudrevatykh, N.V.; Goto, T.: Law of approach to saturation in highly anisotropic ferromagnets application to Nd-Fe-B melt-spun ribbons. J. Alloys Compd. **260**, 196–200 (1997). https://doi.org/10.1016/S0925-8388(97)00127-8

40. Bahrami, A.H.; Sharafi, S.; Baghbaderani, H.A.: The effect of Si addition on the microstructure and magnetic properties of permalloy prepared by mechanical alloying method. Adv. Powder Technol. **24**(1), 235–241 (2013). https://doi.org/10.1016/j.apt.2012.06.008

41. Daza, J.; Mbarek, W.B.; Escoda, L.; Suñol, J.-J.: Characterization and analysis of nanocrystalline soft magnetic alloys: Fe based. Metals. **11**, 1896 (2021). https://doi.org/10.3390/met11121896